Association between lactate metabolism-related molecules and venous thromboembolism: A study based on bioinformatics and an *in vitro* model

ZHONG QIN[1], JING CHEN[1], JIANFENG ZHANG[1], HAILIN LU[1] and QUANZHI CHEN[2]

[1]Department of Vascular Surgery, The First Affiliated Hospital of Guangxi Medical University;
[2]School of Basic Medical Sciences, Guangxi Medical University, Nanning, Guangxi 530021, P.R. China

Received September 26, 2023; Accepted November 22, 2023

DOI: 10.3892/etm.2023.12359

Abstract. Venous thromboembolism (VTE) is characterized by a high recurrence rate and adverse consequences, including high mortality. Damage to vascular endothelial cells (VECs) serves a key role in VTE and lactate (LA) metabolism is associated with VEC damage. However, the pathogenesis of VTE and the role of lactate metabolism-related molecules (LMRMs) remain unclear. Based on the GSE48000 dataset, the present study identified differentially expressed (DE-)LMRMs between healthy individuals and those with VTE. Thereafter, LMRMs were used to establish four machine learning models, namely, the random forest, support vector machine and generalized linear model (GLM) and eXtreme gradient boosting. To verify disease prediction efficiency of the models, nomograms, calibration curves, decision curve analyses and external datasets were used. The optimal machine learning model was used to predict genes involved in disease and an *in vitro* oxygen-glucose deprivation (OGD) model was used to detect the survival rate, LA levels and LMRM expression levels of VECs. A total of four DE-LMRMs, solute carrier family 16 member 1 (SLC16A1), SLC16A7, SLC16A8 and SLC5A12 were obtained and GLM was identified as the best performing model based on its ability to predict differential expression of the embigin, lactate dehydrogenase B, SLC16A1, SLC5A12 and SLC16A8 genes. Additionally, SLC16A1, SLC16A7 and SLC16A8 served key roles in VTE and the OGD model demonstrated a significant decrease in VEC survival rate as well as a significant increase and decrease in intracellular LA and SLC16A1 expression levels in VECs, respectively. Thus, LMRMs may be involved in VTE pathogenesis and be used to build accurate VTE prediction models. Further, it was hypothesized that the observed increase in intracellular LA levels in VECS was associated with the decrease in SLC16A1 expression. Therefore, SLC16A1 expression may be an essential target for VTE treatment.

Correspondence to: Professor Quanzhi Chen, School of Basic Medical Sciences, Guangxi Medical University, 22 Shuangyong Road, Nanning, Guangxi 530021, P.R. China
E-mail: quanzhi_chen@163.com

Professor Zhong Qin, Department of Vascular Surgery, The First Affiliated Hospital of Guangxi Medical University, Guangxi Medical University, 6 Shuangyong Road, Nanning, Guangxi 530021, P.R. China
E-mail: xgwk5632762@tom.com

Key words: venous thromboembolism, vascular endothelial cell, lactate, lactate metabolism-related molecule, solute carrier family 16 member 1

Introduction

Venous thromboembolism (VTE) and its complications are common causes of death worldwide; 30% of patients with VTE die <30 days after diagnosis (1). Additionally, one-third of the remaining 70% of patients experience relapse within 10 years and have long-term complications, including deep vein thrombosis post-thrombotic and post-pulmonary embolism syndrome, chronic thromboembolic pulmonary hypertension in pulmonary embolism and death (2,3). Pro- and antithrombotic factors exist in the human body and an imbalance between these, such as decreases in the levels of antithrombotic factors and/or increases in the levels of prothrombotic factors, may serve key roles in thrombosis (4). However, the mechanisms underlying this imbalance remain unclear. To predict and diagnose VTE, it is necessary to understand the mechanisms underlying its pathogenesis and to construct accurate and effective diagnosis and prediction models.

Vascular endothelial cells (VECs) serve key roles in VTE pathogenesis. Previous studies have reported that VTE causes VEC injury, the accumulation of inflammatory substances, blood hypercoagulation and aggravated thromboembolism, which lead to severe health consequences (5-7). Damage to VECs may disrupt the integrity of blood vessels and lead to bleeding, which affects therapeutic efficacy in VTE (8). In addition to damage caused by the accumulation of inflammatory substances, lactate (LA) may serve an important role in VEC damage (9,10). LA metabolism is regulated by LA metabolism-related molecules (LMRMs). VECs take up glucose from peripheral blood and, via the catalytic activity of various enzymes, such as glycogen and pyruvate kinase,

convert glucose to tricarboxylic acid. This serves as an energy source for cells and pyruvate can also be converted to LA by lactic acid dehydrogenase A (LDHA) (11-14). However, LA does not provide energy to cells but must first be converted by LDHB to pyruvate, which can then be used as a substrate in the tricarboxylic acid cycle (15). LA in VECs is primarily excreted through monocarboxylic acid transporter (MCT) 1 (12) and Stabenow *et al* (16) reported that an increase in LA levels promotes VEC aging, which may be associated with increased conversion of pyruvate to LA by LDHA. Franczyk *et al* (17) suggested that abnormal LA metabolism may be associated with VTE. Additionally, VTE can lead to glucose and oxygen deficiency in local VECs, which can cause changes in levels of metabolic substances, including LA, which serves an important role in VTE (17,18). However, the roles of LA metabolism and LMRMs in the mechanisms underlying VTE remain unclear.

Therefore, the present study screened differentially expressed LMRMs (DE-LMRMs) in patients with VTE and constructed a disease prediction model for VTE to the end of clarifying the roles of LA metabolism and LMRMs in VTE pathogenesis. Further, the oxygen-glucose deprivation (OGD) model of VECs and an *in vitro* model of thromboembolism (19,20) were used to verify the expression of the DE-LMRMs. The present study may provide a novel future target for VTE diagnosis and treatment.

Materials and methods

Data acquisition, preprocessing and screening of DE-LMRMs. The datasets were downloaded from the Gene Expression Omnibus, which is an open-access database with gene chips and high-throughput sequencing datasets (ncbi.nlm.nih.gov/geo). The downloaded datasets included GSE48000 (accession no. GPL10558) and GSE19151 (accession no. GPL571; Fig. 1). GSE48000 training set comprised 25 peripheral blood samples from healthy individuals (control) and 107 peripheral blood samples from patients with VTE (VTE group). The validation set GSE19151 comprised 63 peripheral blood samples from healthy individuals and 70 samples from patients with VTE. The datasets were pre-processed using Perl programming language. Furthermore, LMRMs were obtained from the MsigDB database (version 7.0; gsea-msigdb.Org/gsea/msigdb/). As described by Li *et al* (21), the 'limma' R package was used to screen DE-LMRMs from the GSE48000 dataset and the 'ggpubr' and 'pheatmap' R packages were used to generate box plots and heatmaps, respectively. Finally, 'corrplot' R package was used for correlation analysis(Pearson's coefficient) of the DE-LMRMs. Perl programming language (version 5.30.0.1, URL: https://www.perl.org/) and 'RCircos' package were used to determine the location of the LMRMs on chromosomes.) and R programming language (version 4.1.3, URL: https://www.r-project.org/) was employed to conduct this study.

Construction of predictive model using machine learning methods. Based on screened LMRMs, the 'caret' R package was used to build machine learning models, namely, the random forest (RF), support vector machine (SVM) and generalized linear model (GLM) and eXtreme Gradient Boosting (XGB) (21). The 'DALEX' R package was used to interpret the four models and generate the residual distribution of each model in the test set. The 'pROC' R package was used to visualize the area under the receiver operating characteristic (ROC) curve (AUC). Next, the optimal machine learning model was identified. The model with highest AUC was considered the optimal model. The top five variables were considered key predictor genes associated with VTE. ROC curve analysis of the GSE48000 dataset was performed to verify the diagnostic value of the model.

Construction and validation of the nomogram model. Using the 'rms' R package, nomogram models were constructed to evaluate VTE clusters. Each predictor had a corresponding score and 'total score' represented the sum of the individual scores of all the predictors. Calibration curve and decision curve analysis (DCA) were used to estimate the predictive power of the nomogram model.

Establishment of the OGD model. The OGD model is an *in vitro* thromboembolic model (19,20). Human umbilical (HU)VECs were purchased from Shanghai Anwei Biotechnology Co., Ltd. (cat. no. HUVEC-SV40T). Mycoplasma testing was performed on HUVECs and the cell line was authenticated using immunofluorescence. Cells were cultured in RPMI-1640 medium (cat. no. 22400097) with 10% fetal bovine serum (cat. no. 12483020) and 1% penicillin-streptomycin (cat. no. 15140122; all Gibco; Thermo Fisher Scientific, Inc.) in a humidified incubator at 37˚C with 5% CO_2 and 95% air for 7 days. Cells ($1.5x10^5$/ml) were transferred to a 6-well plate in glucose-free DMEM (cat. no. 119660-25; Gibco; Thermo Fisher Scientific, Inc.) and cultured for 24 h in a humidified incubator at 37˚C with 5% CO_2 and 95% N_2. Cell morphology was observed using a light microscope (magnification, x200; cat. no. D-35578; Leica Microsystems GmbH).

MTT analysis of VEC survival rate. VEC survival was analyzed as described by Li *et al* (22) using the MTT kit (cat. no. AR1156; Wuhan Boster Biotechnology, Ltd.). MTT staining solution (10 μl) was added to each well and incubated at 37˚C for 4 h. Next, 100 μl formazan as added to each well and samples were incubated at 37˚C for 4 h. Absorbance was measured at 570 nm using an enzyme-labeled instrument.

Detection of LA levels. Total protein was extracted from VECs using a protein extraction kit (cat. no. SD-001/SN-002; Invent Biotechnologies Inc.). BCA assay kit (cat. no. P0012S; Beyotime Institute of Biotechnology) was used to evaluate total protein concentration levels. LA content assay kit (cat. no. BC2235; Beijing Solarbio Science & Technology Co., Ltd.) was used to measure the LA levels, as previously described (23,24).

Western blotting analysis. Samples (20 μg protein/lane) were obtained as aforementioned and separated using SDS-PAGE (12.5%) and transferred onto nitrocellulose (NC) membranes (MilliporeSigma)usingwettransfercell(Bio-RadMini-Protean 1658001, Bio-Rad Laboratories, Inc.). NC membranes were blocked with 5% BSA blocking buffer (cat. no. SW3015, Solarbio Science & Technology Co., Ltd.) for 1 h at 25˚C and incubated overnight with primary antibodies at 4˚C. The

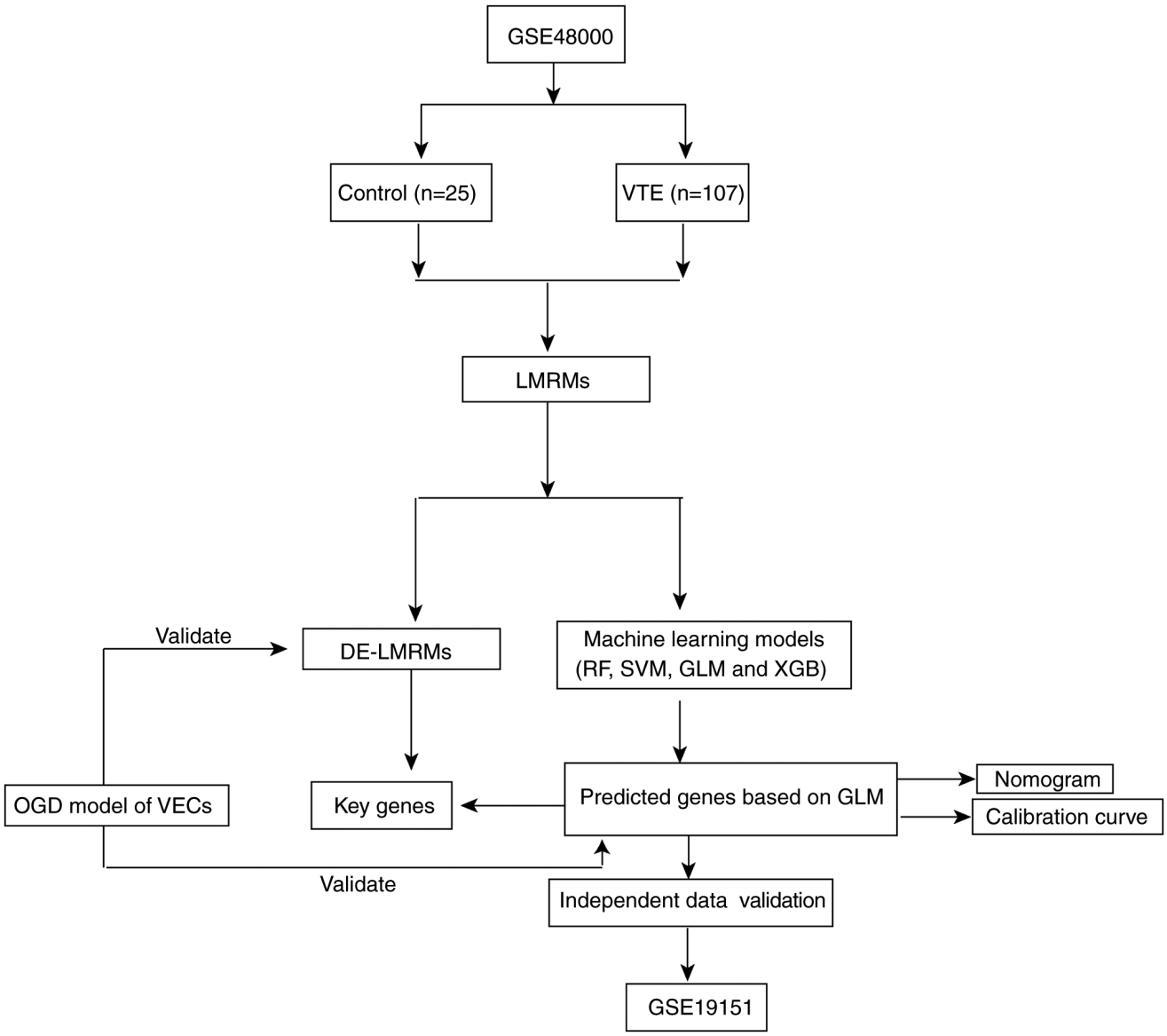

Figure 1. Experimental design. DE-LMRM, differentially expressed lactate metabolism-related molecule; VTE, venous thromboembolism; RF, random forest; SVM, support vector machine; GLM, generalized linear model; XGB, eXtreme Gradient Boosting; VEC, venous endothelial cell.

primary antibodies were as follows: Anti-monocarboxylic acid transporter (MCT)1 (cat. no. ab85021; 1:1,000; Abcam), anti-embigin (EMB; cat. no. ab170927; 1:1,000: Abcam), anti-MCT2 (cat. no. ab81262; 1:400; Abcam), anti-LDHB (cat. no. ab264358; 1:2,000; Abcam), anti-solute carrier family 5 member 12 (SLC5A12; cat. no. sc-515141; 1:800; Santa Cruz Biotechnology, Inc.), anti-SLC16A8 (cat. no. D262213; 1:1,000; Sangon Biotech Co., Ltd.) and anti-GAPDH (cat. no. D110016; 1:10,000; Sangon Biotech Co., Ltd.). NC membranes were incubated with horseradish peroxidase-conjugated Affinipure goat anti-rabbit IgG (H+L) antibody (cat. no. SA00001-2; 1:8,000; Proteintech Group, Inc.) for 1 h at 25˚C. Further, immunoreactive bands were visualized using the Omni-ECL™ Femto Light Chemiluminescence kit (cat. no. SQ201; EpiZyme) and ChemiScope6000 (Clinx) visualization system. Band intensities were quantified used ImageJ software (version: 1.8.0, National Institutes of Health). The total protein levels were normalized to GAPDH.

Statistical analysis. All statistical analysis was performed using SPSS software (version 25.0; IBM Corp.). Data are expressed as the mean ± standard deviation (n=6). Unpaired independent sample t-test was performed to analyze differences between groups. $P<0.05$ was considered to indicate a statistically significant difference.

Results

Identification of DE-LMRMs in VTE. The location of the LMRMs on chromosomes was determined (Fig. 2A). The 'limma' package in R was used to screen DE genes from the dataset(GSE48000) (21). Compared with the control, four DE-LMRMs (SLC16A1, SLC16A7), SLC16A8 and SLC5A12) were identified in the VTE group. Specifically, SLC16A1 demonstrated decreased expression, whereas SLC16A7, SLC16A8 and SLC5A12 demonstrated increased expression in the VTE group compared with the control group (Fig. 2B and C). Correlation analysis was used to analyze correlations

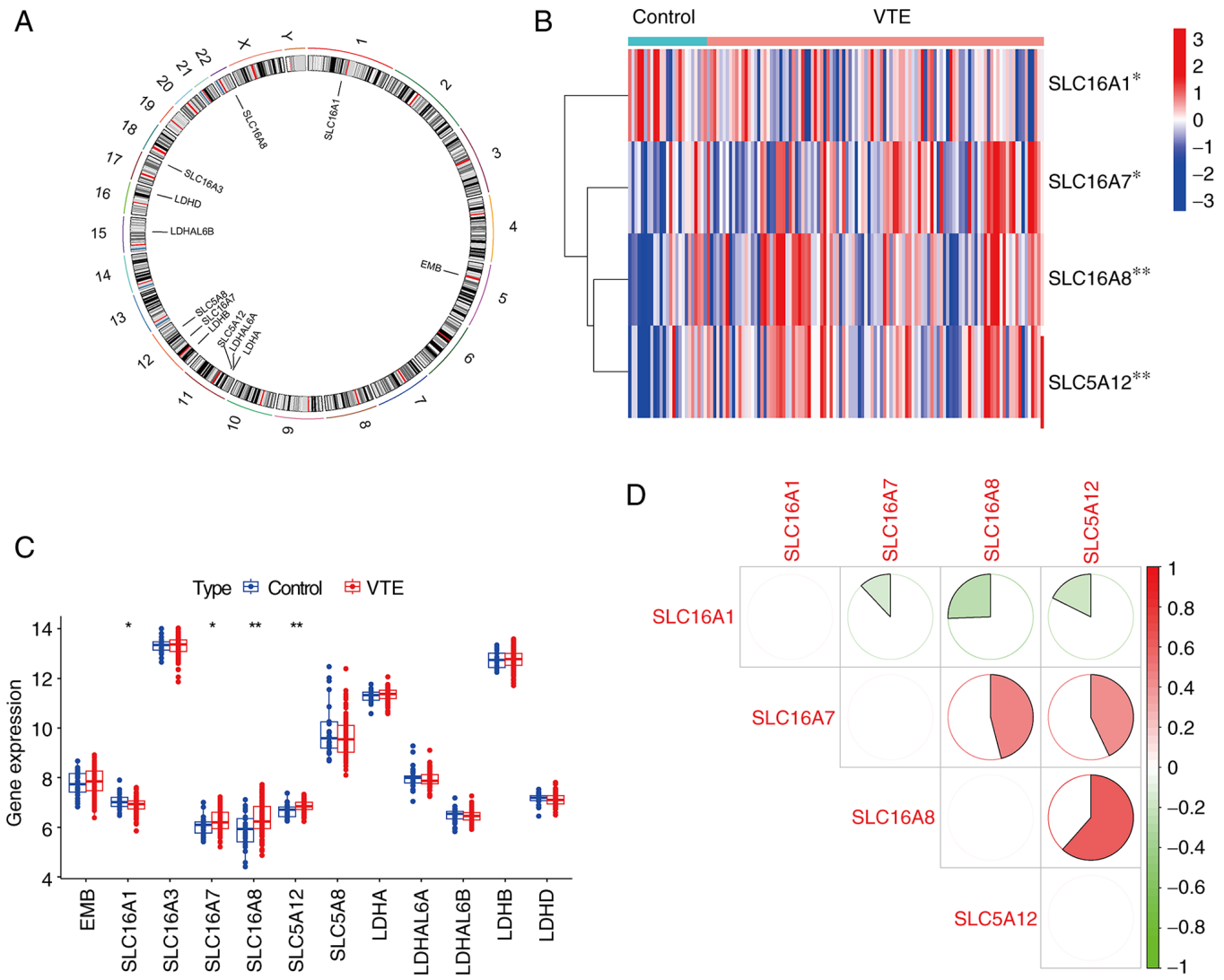

Figure 2. LMRMs in GSE48000 dataset. (A) Location of LMRMs on chromosomes. (B) Heatmap of expression levels of DE-LMRMs. (C) Boxplot of expression levels of four DE-LMRMs. (D) Correlation analysis between DE-LMRMs. Red, positive; green, negative. *P<0.05, **P<0.01 vs. control. DE-LMRM, differentially expressed lactate metabolism-related molecule; VTE, venous thromboembolism; SLC16A1, solute carrier family 16 member 1; EMB, embigin; LDHD, lactate dehydrogenase D; LDHAL6B, LDHA-like 6B.

between the four DE-LMRMs. Significant positive correlations were found between SLC16A7 and SCL16A8, SLC16A7 and SCL5A12, SLC16A8 and SCL5A12. Significant negative correlations were found SLC16A1 and SLC16A7, SCL16A1 and SLC16A8, SLC16A1 and SLC5A12 (Fig. 2D).

Construction and assessment of machine learning models. A total of four machine learning models (RF, SVM, GLM and XGB) were constructed based on expression levels of LMRMs. GLM and XGB machine learning models demonstrated relatively low residuals (Fig. 3A and B). Discriminative performances of the four machine learning algorithms were evaluated by generating ROC curves based on five-fold cross-validation in the GSE48000 training dataset (Fig. 3C). The AUCs were as follows: RF=0.440, SVM=0.759, XGB=0.674 and GLM=0.728. Based on the residual and AUC values, the GLM machine learning model was optimal with respect to distinguishing patients with VTE. The five most important genes (EMB, LDHB, SLC16A1, SLC5A12 and SLC16A8) determined by this model were selected as predictor genes for further analysis. Finally, the GSE19151 dataset was used to verify the accuracy of the machine learning model. In the GSE152532 dataset, the ROC curve for the GLM gene prediction model performed well, with AUC=0.513 (Fig. 3D).

Construction of the nomogram model. A nomogram integrates multiple prediction indicators based on multi-factor regression analysis (27). A nomogram model was constructed to estimate VTE risk (Fig. 4A). The calibration curve and DCA were used to evaluate the prediction efficiency of the nomogram model. Based on the calibration curve, the error between the actual and predicted risks for the VTE cluster was low (Fig. 4B). DCA indicated that the nomogram was accurate (Fig. 4C). To facilitate the clinical use of this diagnostic model, a nomogram was constructed. Based on the actual measured values of expression levels of the five DE-LMRMs in the blood of patients with VTE, it was possible to find these DE-LMRMs on the corresponding scale in the nomogram and project to the

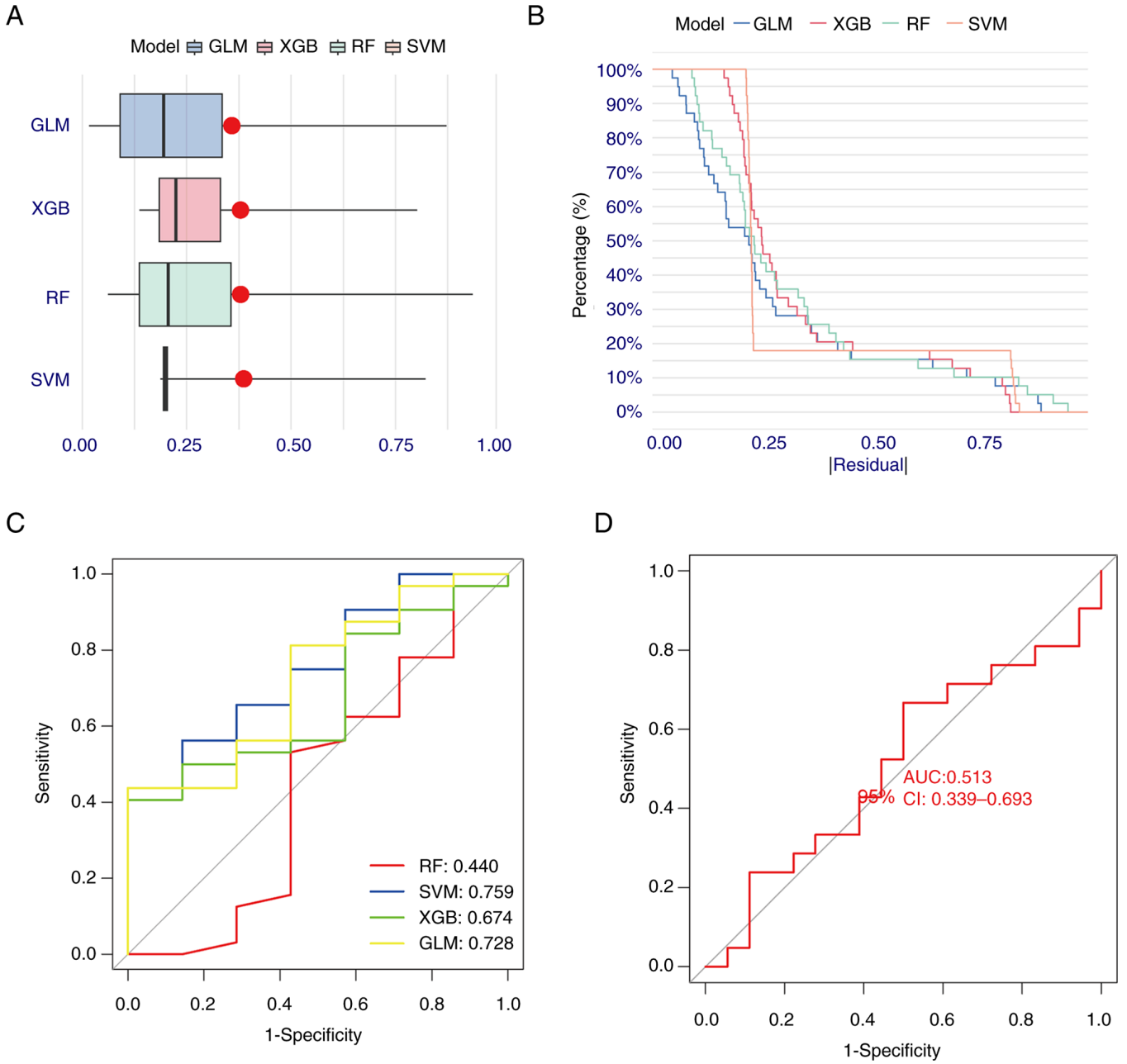

Figure 3. Machine learning models in GSE48000 dataset. Residual distribution for machine learning models presented as (A) boxplots and (B) reverse cumulative distribution. (C) ROC analysis of machine learning models based on five-fold cross-validation in the test cohort. AUCs were obtained for the four models. (D) ROC curve of five genes of the GLM model, which showed optimal performance. AUC, area under the curve; ROC, receiver operating characteristic; RF, random forest; SVM, support vector machine; GLM, generalized linear model; XGB, eXtreme gradient boosting.

point scale on top to read the value for each variant. The total number of points was obtained by summing the individual points and the risk probability for a patient with VTE could be estimated using the bottom scale by projecting the total.

Survival rate, LA levels and expression of LMRMs in the OGD model. Compared with the control, the OGD model showed a lower number of VECs and these VECs appeared swollen and ruptured (Fig. 5A). MTT is a cell viability assay that involves conversion of the water-soluble yellow dye MTT to insoluble purple formazan by the action of mitochondrial reductase (28). MTT assay demonstrated a significant decrease in the survival rate of the VECs in the OGD compared with the control. Compared with control group, the survival rate significantly decreased to 52.49±5.17% in the OGD group (Fig. 5B). Furthermore, compared with the control, the OGD VECs demonstrated significantly higher LA levels (37.38±4.18 vs. 75.90±4.21 μmol/mg protein, respectively; Fig. 5C). Based on the genes predicted using the GLM model and DE-LMRMs, three key molecules (SLC16A1, SLC5A12 and SLC16A8) were identified (Fig. 5D). Additionally, western blotting to detect the protein expression levels of EMB, LDHB, SLC16A1, SCL16A7, SLC5A12 and SLC16A8 in VECs demonstrated that the protein expression of SLC16A1 significantly decreased to 49.69±2.55% in the OGD group (Fig. 5E), while the protein expression levels of the other five molecules demonstrated no significant change (Fig. 5E).

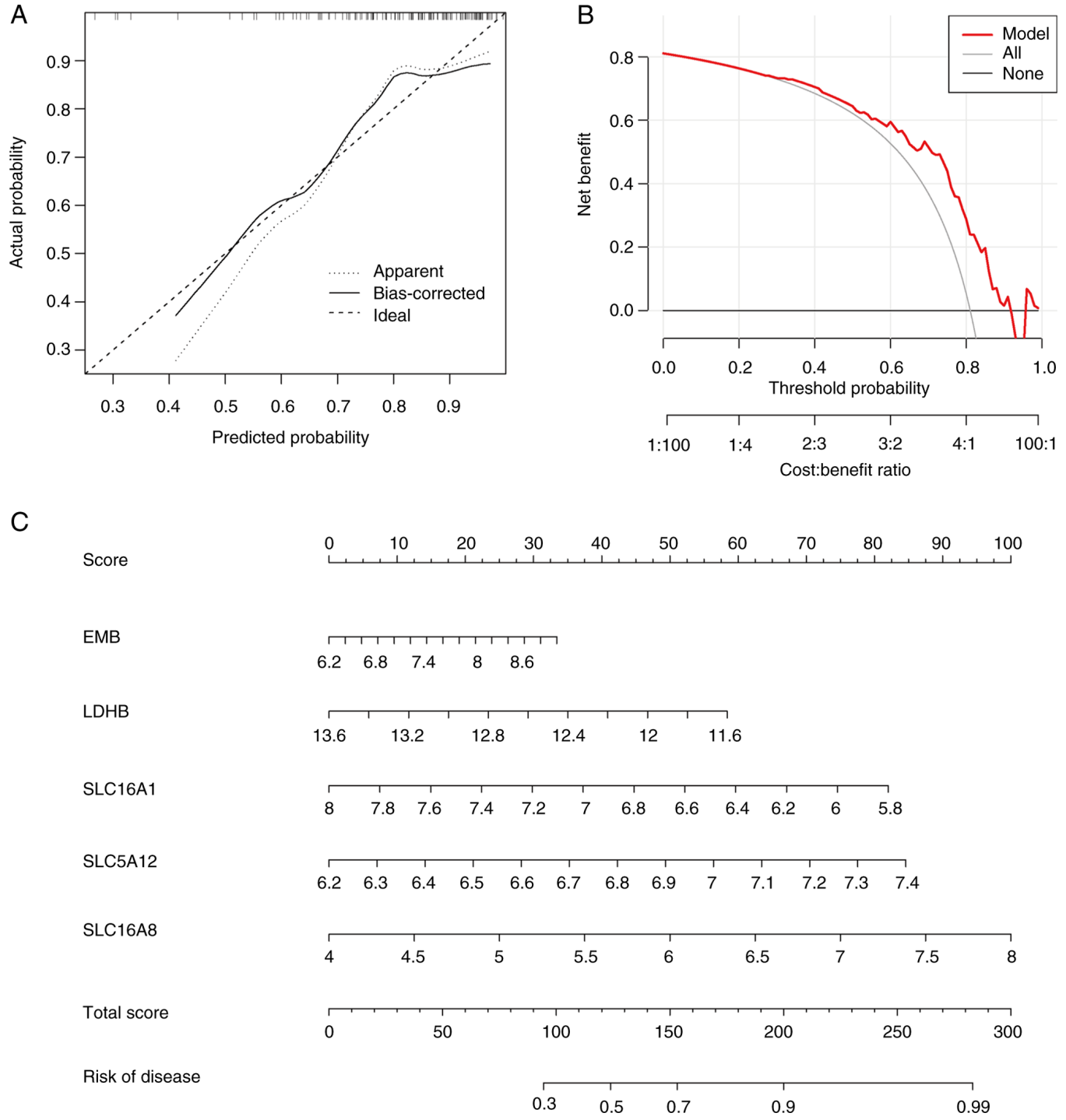

Figure 4. Nomogram models in GSE48000 dataset. (A) Nomogram for predicting risk of VTE based on the five-gene-based generalized linear model. (B) Calibration and (C) decision curve analysis showed relatively high accuracy for the nomogram. EMB, embigin; LDHB, lactate dehydrogenase B; SLC16A1, solute carrier family 16 member 1.

Discussion

Although it has previously been reported that an imbalance between prothrombotic and antithrombotic factors serves a key role in VTE pathogenesis (4), the associated mechanisms remain unclear. It has been suggested that an imbalance in levels of several metabolic substances in the blood may also be associated with VTE pathogenesis (17). Among these, LA serves an important role in VEC damage (9,10). VECs obtain glucose from blood and convert it to ATP to supply cells with energy (11-14). VTE can cause ischemia and hypoxia of local blood vessels that can result in glucose and oxygen deficiency in VECs, which may lead to energy metabolism disorder. If these are not corrected, cell damage can occur (22). It has also been reported that in energy metabolism disorder, the accumulation of large amounts of LA serves a key role in cell function and structural damage (9).

Additionally, intracellular LA, which is primarily regulated by LMRMs, is associated with LA production, consumption

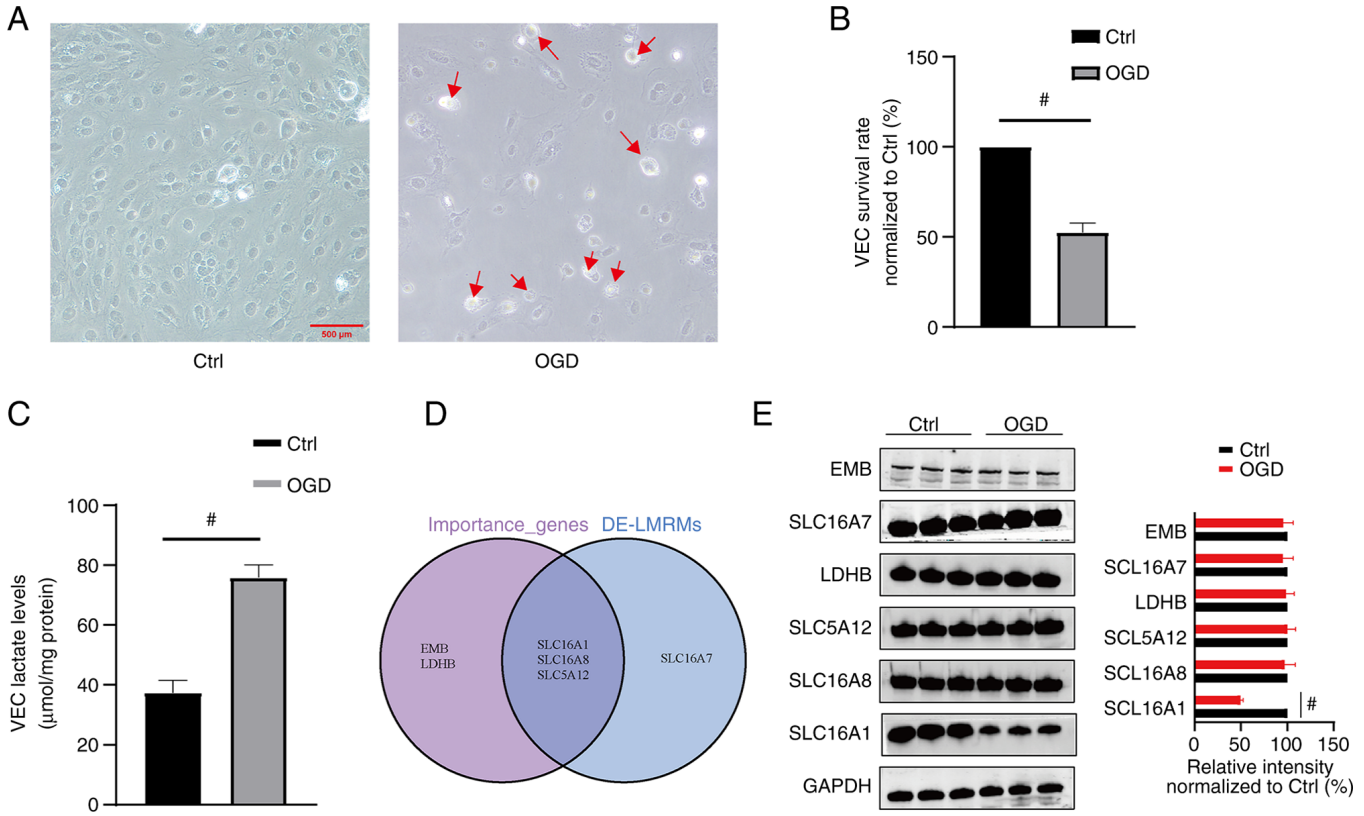

Figure 5. Experimental Analyses for the OGD model (A) Morphology analysis of VECs showed a lower number of VECs in the OGD compared with the Ctrl group. The VECs in the OGD appeared swollen and ruptured. Magnification, x200. Red arrows: swollen and ruptured VECs. (B) MTT results demonstrated a significantly lower VEC survival rate in the OGD group compared with the Ctrl group. (C) Significantly increased VEC lactate levels were shown in the OGD compared with the Ctrl group. (D) A total of three key molecules in VTE pathogenesis were obtained using prediction genes of the GLM model and DE-LMRMs. (E) Western blotting analysis demonstrated significantly decreased MCT1 protein expression in the OGD group (n=6). #P<0.01 vs. Ctrl. Ctrl, control; OGD, oxygen-glucose deprivation; VEC, vascular endothelial cell; LDHB, lactic acid dehydrogenase B; EMB, embigin; SCL16A1, solute carrier family 16 member 1; DE-LMRM, differentially expressed lactate metabolism-related molecule.

and transport (11-14). In the present study, LMRMs from the MsigDB database were screened and DE-LMRMs were identified by comparing gene expression between healthy individuals and patients with VTE. A total of four DE-LMRMs were identified in the VTE group, with SLC16A1 demonstrating decreased expression levels, whereas SLC16A7, SLC16A8 and SLC5A12 demonstrated increased expression. Reportedly, these DE-LMRMs are primarily responsible for LA transport (12,26), which suggests that abnormal LA transport may be involved in VTE pathogenesis. Machine learning models have previously been used to predict prevalence of a number of diseases, with lower error rates and superior results compared with conventional logistic regression (27). Machine learning models, such as RF, SVM, GLM and XGB, demonstrate clinical relevance in disease prediction (21). In the present study, machine learning models based on the expression of the LMRMs were constructed. After comparing AUC values corresponding to the four models, GLM was identified as the optimal model and its verification using external data indicated that it demonstrated relatively good accuracy in predicting VTE. The five predicted genes in GLM were EMB, LDHB, SLC16A1, SLC5A12 and SLC16A8. DCA indicated that the nomogram could potentially provide a basis for clinical decision-making EMB is a companion protein located on the cell membrane that promotes localization of MCT1 to the plasma membrane and alters transport of LA by MCT1 (28). LDH is a homologous or heterotetrametric enzyme with two subunits, LDHA and LDHB, which are encoded by different genes and have different chromosomal locations. LDHA is located on chromosome 11, while LDHB is primarily located on chromosome 12 (13,29). LDHA preferentially converts pyruvate to LA, whereas LDHB converts LA to pyruvate (15,30,31). The present study demonstrated that LDHB was an important gene for predicting VTE, which suggested that intracellular LA conversion may be involved in VTE pathogenesis.

VTE pathogenesis is a complex process and its simulation using *in vivo* as well *in vitro* models remains challenging. *In vivo* models of venous thrombosis are primarily established via ferric chloride administration (32,33); in *in vitro* models, in which cells are deprived of glucose and oxygen, the cells are in a state of hypoxia and sugar deficiency (19,20,34). VTE also causes local blood vessel ischemia and hypoxia, which results in ECs in these blood vessels being in a state of glucose and oxygen deprivation. Hence, the OGD model only partially simulates thromboembolism (19,20). In the present study, OGD was used to verify the association between LA, LMRMs and VTE. Light microscopy demonstrated a decrease in number of VECs and edema in the OGD model compared with control cells. A significant decrease in the survival rate of VECs in the OGD group compared with the control was shown and the intracellular LA

levels increased significantly. This suggested that cell survival was negatively associated with intracellular LA. Additionally, more obvious cell damage and a lower cell survival rate was observed at higher LA levels. According to the GLM-predicted genes and DE-LMRMs, three molecules, SLC16A1, SLC16A7 and SLC16A8, were identified as key in VTE pathogenesis. Western blotting was employed to detect the expression levels of the proteins encoded by DE-LMRMs and GLM-predicted genes. The expression of SLC16A1 was significantly decreased in the OGD group, consistent with the prediction results. Further, MCT1, which is encoded by SLC16A1, is primarily expressed in VECs (12) and decreased SLC16A1 expression may limit excretion of intracellular LA, which results in an increase in intracellular LA levels, cell acidification and impaired cell function (35). The expression levels of proteins encoded by EMB, LDHB, SCL16A7, SLC5A12 and SLC16A8 did not change significantly in the OGD compared with the control group. EMB, a companion protein of MCT1, primarily regulates the expression of MCT1 on cell membrane (28). The expression of LDHB did not change significantly, which suggested that LA conversion to pyruvate was not affected in the OGD group. SLC16A7, which encodes the MCT2 protein, is primarily expressed in the brain (36). SLC5A12, which encodes sodium-coupled monocarboxylate transporter 2 (SMCT2), is primarily expressed in the kidney (37) and SLC16A8, which encodes MCT3, is primarily expressed in the retina (38). The aforementioned reports suggest that EMB, LDHB, SLC16A7, SLC5A12 and SLC16A8 do not serve key roles in LA metabolism in VECs.

The present study had a number of limitations. The *in vitro* OGD model cannot completely simulate VTE, therefore, it is necessary to collect clinical samples and build an *in vivo* model for further studies on VTE.

In the present study, it was demonstrated that LMRMs may participate in VTE pathogenesis. Thus, a prediction model was developed and showed a certain degree of accuracy. Model-predicted results were verified using an *in vitro* model, which confirmed that an increase in intracellular LA levels may be associated with a decrease in SLC16A1 expression. In summary, LMRMs, particularly SLC16A1, may serve key roles in VTE pathogenesis and be a potential target for VTE diagnosis and treatment.

Acknowledgements

Not applicable.

Funding

The present study was supported by Guangxi Key Research and Development Plan (grant. no. 2017AB45033)

Availability of data and materials

The datasets used and/or analyzed during the current study are available from the corresponding author on reasonable request.

Authors' contributions

ZQ wrote the manuscript, performed the experiments and analyzed the data. JC performed cellular experiments. JZ and HL contributed to the design of this study and involved in proof reading and editing. QC contributed to acquisition of data and data interpretation. HL and QC confirm the authenticity of all the raw data. ZQ and QC provided the funding and supervised the study. All authors read and approved the final manuscript.

Ethics approval and consent to participate

Not applicable.

Patient consent for publication

Not applicable

Competing interests

The authors declare that they have no competing interests.

References

1. Battinelli EM, Murphy DL and Connors JM: Venous thromboembolism overview. Hematol Oncol Clin North Am 26: 345-367, ix, 2012.
2. Bartholomew JR: Update on the management of venous thromboembolism. Cleve Clin J Med 84 (Suppl 3): 39-46, 2017.
3. Klok FA, van der Hulle T, den Exter PL, Lankeit M, Huisman MV and Konstantinides S: The post-PE syndrome: A new concept for chronic complications of pulmonary embolism. Blood Rev 28: 221-226, 2014.
4. Palta S, Saroa R and Palta A: Overview of the coagulation system. Indian J Anaesth 58: 515-523, 2014.
5. Torres C, Matos R, Morais S, Campos M and Lima M: Soluble endothelial cell molecules and circulating endothelial cells in patients with venous thromboembolism. Blood Coagul Fibrinolysis 28: 589-595, 2017.
6. Pilard M, Ollivier EL, Gourdou-Latyszenok V, Couturaud F and Lemarié CA: Endothelial cell phenotype, a major determinant of venous thrombo-inflammation. Front Cardiovasc Med 9: 864735, 2022.
7. Poredos P and Jezovnik MK: The role of inflammation in venous thromboembolism and the link between arterial and venous thrombosis. Int Angiol 26: 306-311, 2007.
8. Barsh GS, Molina-Ortiz P, Orban T, Martin M, Habets A, Dequiedt F and Schurmans S: Rasa3 controls turnover of endothelial cell adhesion and vascular lumen integrity by a Rap1-dependent mechanism. PLoS Genet 14: e1007195, 2018.
9. Yang K, Fan M, Wang X, Xu J, Wang Y, Gill PS, Ha T, Liu L, Hall JV, Williams DL and Li C: Lactate induces vascular permeability via disruption of VE-cadherin in endothelial cells during sepsis. Sci Adv 8: eabm8965, 2022
10. Yang K, Holt M, Fan M, Lam V, Yang Y, Ha T, Williams DL, Li C and Wang X: Cardiovascular dysfunction in covid-19: Association between endothelial cell injury and lactate. Front Immunol 13: 868679, 2022.
11. Mamun AA, Hayashi H, Yamamura A, Nayeem MJ and Sato M: Hypoxia induces the translocation of glucose transporter 1 to the plasma membrane in vascular endothelial cells. J Physiol Sci 70: 44, 2020.
12. Shao H and Li S: A new perspective on HIV: Effects of HIV on brain-heart axis. Front Cardiovasc Med 10: 1226782, 2023.
13. Edwards YH, Povey S, LeVan KM, Driscoll CE, Millan JL and Goldberg E: Locus determining the human sperm-specific lactate dehydrogenase, LDHC, is syntenic with LDHA. Dev Genet 8: 219-232, 1987.
14. Mdluli K, Booth MP, Brady RL and Rumsby G: A preliminary account of the properties of recombinant human glyoxylate reductase (GRHPR), LDHA and LDHB with glyoxylate, and their potential roles in its metabolism. Biochim Biophys Acta 1753: 209-216, 2005.
15. Koukourakis MI, Giatromanolaki A, Sivridis E, Bougioukas G, Didilis V, Gatter KC and Harris AL; Tumour and Angiogenesis Research Group: Lactate dehydrogenase-5 (LDH-5) overexpression in non-small-cell lung cancer tissues is linked to tumour hypoxia, angiogenic factor production and poor prognosis. Br J Cancer 89: 877-885, 2003.

16. Stabenow LK, Zibrova D, Ender C, Helbing DL, Spengler K, Marx C, Wang ZQ and Heller R: Oxidative glucose metabolism promotes senescence in vascular endothelial cells. Cells 11: 2213, 2022.
17. Franczyk B, Gluba-Brzózka A, Ławiński J, Rysz-Górzyńska M and Rysz J: Metabolomic profile in venous thromboembolism (VTE). Metabolites 11: 495, 2021.
18. Lim CS, Kiriakidis S, Sandison A, Paleolog EM and Davies AH: Hypoxia-inducible factor pathway and diseases of the vascular wall. J Vasc Surg 58: 219-230, 2013.
19. Li WQ, Qin ZS, Chen S, Cheng D, Yang SC, Choi YMM, Chu B, Zhou WH and Zhang ZJ: Hirudin alleviates acute ischemic stroke by inhibiting NLRP3 inflammasome-mediated neuroinflammation: In vivo and in vitro approaches. Int Immunopharmacol 110: 108967, 2022.
20. Wang Z, Liu P, Hu M, Lu S, Lyu Z, Kou Y, Sun Y, Zhao X, Liu F and Tian J: Naoxintong restores ischemia injury and inhibits thrombosis via COX2-VEGF/ NFκB signaling. J Ethnopharmacol 270: 113809, 2021.
21. Li S, Long Q, Nong L, Zheng Y, Meng X and Zhu Q: Identification of immune infiltration and cuproptosis-related molecular clusters in tuberculosis. Front Immunol 14: 1205741, 2023.
22. Li S, Zheng Y, Long Q, Nong J, Shao H, Liang G and Wu F: Drug-drug interactions between propofol and ART drugs: Inhibiting neuronal activity by affecting glucose metabolism. CNS Neurosci Ther: Aug 31, 2023 (Epub ahead of print).
23. Xie X, Hu Y, Ye T, Chen Y, Zhou L, Li F, Xi X, Wang S, He Y, Gao X, *et al*: Therapeutic vaccination against leukaemia via the sustained release of co-encapsulated anti-PD-1 and a leukaemia-associated antigen. Nat Biomed Eng 5: 414-428, 2020.
24. Wang S, Zhou L, Ji N, Sun C, Sun L, Sun J, Du Y, Zhang N, Li Y, Liu W, *et al*: Targeting acyp1-mediated glycolysis reverses lenvatinib resistance and restricts hepatocellular carcinoma progression. Drug Resist Updat, 69: 100976, 2023.
25. Kumar P, Nagarajan A and Uchil PD: Analysis of cell viability by the MTT assay. Cold Spring Harb Protoc 2018: 2018.
26. Sivaprakasam S, Bhutia YD, Yang S and Ganapathy V: Short-chain fatty acid transporters: Role in colonic homeostasis. Compr Physiol 8: 299-314, 2017.
27. Zhao X, Lu Y, Li S, Guo F, Xue H, Jiang L, Wang Z, Zhang C, Xie W and Zhu F: Predicting renal function recovery and short-term reversibility among acute kidney injury patients in the ICU: Comparison of machine learning methods and conventional regression. Ren Fail 44: 1327-1338, 2022.
28. Xu B, Zhang M, Zhang B, Chi W, Ma X, Zhang W, Dong M, Sheng L, Zhang Y, Jiao W, *et al*: Embigin facilitates monocarboxylate transporter 1 localization to the plasma membrane and transition to a decoupling state. Cell Rep 40: 111343, 2022.
29. Li SS, Luedemann M, Sharief FS, Takano T and Deaven LL: Mapping of human lactate dehydrogenase-A -B and -C genes and their related sequences: the gene for LDHC is located with that for LDHA on chromosome 11. Cytogenet Cell Genet 48: 16-18, 1988.
30. Markert CL, Shakle JB and Whitt GS: Evolution of a gene. Multiple genes for LDH isozymes provide a model of the evolution of gene structure, function and regulation. Science 189: 102-114, 1975.
31. Swiderek K and Paneth P: Differences and similarities in binding of pyruvate and L-lactate in the active site of M4 and H4 isoforms of human lactate dehydrogenase. Arch Biochem Biophys 505: 33-41, 2011.
32. Srivastava AK, Kalita J, Haris M, Gupta RK and Misra UK: Radiological and histological changes following cerebral venous sinus thrombosis in a rat model. Neurosci Res 65: 343-346, 2009.
33. Song W, Ci H, Tian G, Zhang Y and Ge X: Edoxaban improves venous thrombosis via increasing hydrogen sulfide and homocysteine in rat model. Mol Med Rep 16: 7706-7714, 2017.
34. Zhao Z, Wu C, He X, Zhao E, Hu S, Han Y, Wang T, Chen Y, Liu T and Huang S: Microrna let-7f alleviates vascular endothelial cell dysfunction via targeting HMGA2 under oxygen-glucose deprivation and reoxygenation. Brain Res 1772: 147662, 2021.
35. Benjamin D, Robay D, Hindupur SK, Pohlmann J, Colombi M, El-Shemerly MY, Maira SM, Moroni C, Lane HA and Hall MN: Dual inhibition of the lactate transporters MCT1 and MCT4 is synthetic lethal with metformin due to NAD+ depletion in cancer cells. Cell Rep 25: 3047-3058.e4, 2018.
36. Yu X, Zhang R, Wei C, Gao Y, Yu Y, Wang L, Jiang J, Zhang X, Li J and Chen X: MCT2 overexpression promotes recovery of cognitive function by increasing mitochondrial biogenesis in a rat model of stroke. Anim Cells Syst (Seoul) 25: 93-101, 2021.
37. Srinivas SR, Gopal E, Zhuang L, Itagaki S, Martin PM, Fei YJ, Ganapathy V and Prasad PD: Cloning and functional identification of slc5a12 as a sodium-coupled low-affinity transporter for monocarboxylates (SMCT2). Biochem J 392: 655-664, 2005.
38. Daniele LL, Sauer B, Gallagher SM, Pugh EN Jr and Philp NJ: Altered visual function in monocarboxylate transporter 3 (slc16a8) knockout mice. Am J Physiol Cell Physiol 295: C451-C457, 2008.